JACS
JOURNAL OF THE AMERICAN CHEMICAL SOCIETY
pubs.acs.org/JACS
Article

Proteome-Mining and Chemical Activation of Hidden Bioactive Fragments as Antimicrobial Assemblies

Huayang Liu,[‖] Ziheng Xu,[‖] Yu Zhang, Dinghao Chen, Liheng Lu, Shichao Xu, Jianjun Cheng, and Huaimin Wang*

Cite This: J. Am. Chem. Soc. 2026, 148, 4660−4669
Read Online
ACCESS | Metrics & More | Article Recommendations | Supporting Information

ABSTRACT: Proteolytic processing of precursor proteins liberates bioactive fragments, yet the systematic discovery of such peptides remains challenging. Here, we establish a fragment-mining strategy that combines in silico prediction with chemical tailoring to generate self-assembling antimicrobial peptides directly from protein sequences, including previously unannotated proteins. Self-assembly proved integral to activity: amphiphilic modification promoted nanonet formation and efficient bacterial membrane disruption, while rational glycosylation reprogrammed physicochemical properties to confer selectivity for bacterial phosphatidylglycerol over mammalian phosphatidylcholine, thereby broadening the therapeutic window. The optimized peptide, C_{16}-KA6-Glc, displayed broad-spectrum bactericidal activity, superior biofilm eradication, and negligible resistance development. In murine models of thigh and pneumonia infection, C_{16}-KA6-Glc achieved therapeutic efficacy comparable to that of conventional antibiotics while also attenuating inflammatory responses. These findings demonstrate a generalizable approach to translating latent proteome fragments into *de novo* self-assembling peptide therapeutics with clinical potential.

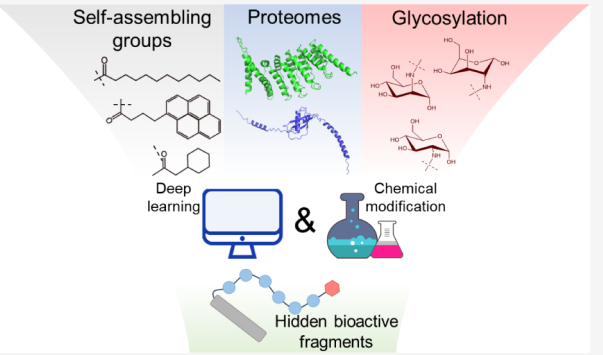

INTRODUCTION

Peptides are widely used by living systems as dynamic regulators of defense, signaling, and metabolism. In many cases, these functional sequences are not encoded as free peptides but are embedded within larger precursor proteins and liberated through enzymatic processing only when needed. This strategy allows organisms to maintain reservoirs of latent functional sequences mobilized under stress or infection. Such regulated release is well documented in classical antimicrobial peptides (AMPs) and hormones, underscoring the central role of proteolysis in peptide biology.[1,2] For example, LL-37 is generated in vivo through proteolytic cleavage of cathelicidin antimicrobial protein (CAP) by proteinase 3 (Figure 1A),[3−5] whereupon it exerts antimicrobial and immunomodulatory activities.[6−8] During the conversion of proinsulin to insulin, proinsulin undergoes sequential proteolytic cleavage by prohormone convertases (PC1/3 and PC2) and carboxypeptidase E,[9,10] ultimately producing mature insulin that regulates blood glucose levels.

Over the past two decades, the scope of AMP diversity has become increasingly apparent across animals, plants, and microbes. These short, often cationic, amphipathic molecules share a unifying ability to disrupt microbial membranes, yet vary widely in sequence, structure, and mechanism.[11,12] Among the mechanisms that enhance their potency, self-assembly has emerged as a key principle: supramolecular organization can stabilize short sequences, promote multivalent interactions, and amplify antimicrobial effects.[13−28] Despite its importance, most peptide discovery strategies have been limited to derivatives of known sequences or random screening, leaving the vast proteome-encoded fragment space largely uncharted.[29] Recent findings highlight both the promise and the challenge of this hidden reservoir. Proteasomes, for instance, have been shown to generate small cationic fragments with direct antimicrobial activity, suggesting that host cells continually produce cryptic defense peptides.[30−32] Computational analyses predict that hundreds of thousands of such latent fragments may exist in the human proteome.[33] Yet, systematically identifying those with emergent behaviors—such as supramolecular assembly, membrane selectivity, and host compatibility—remains an unresolved challenge.

Here, we present an integrated framework to address this problem by coupling deep learning-based fragment mining with supramolecular chemical design (Figure 1B). Using a previously established sequence-assembly predictor (Trans-

Received: November 20, 2025
Revised: January 9, 2026
Accepted: January 13, 2026
Published: January 22, 2026

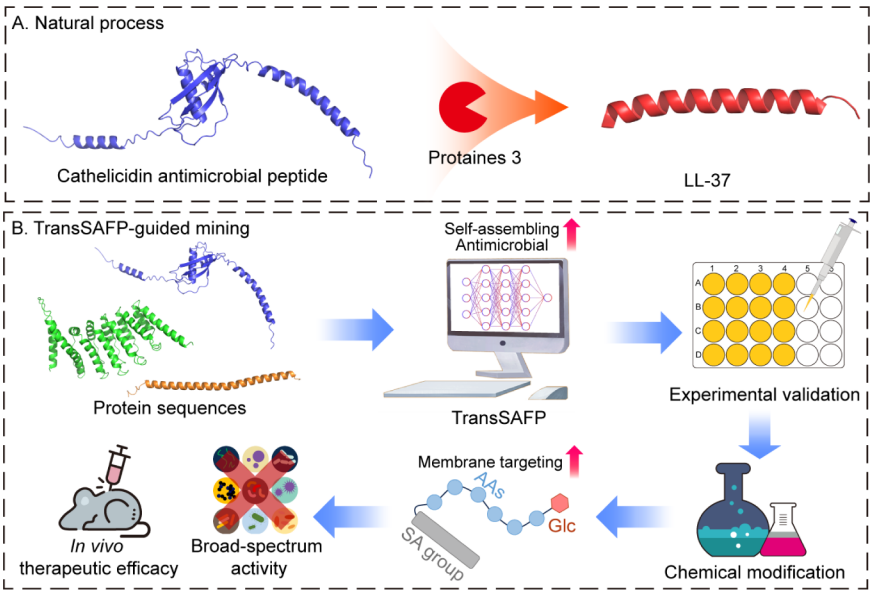

Figure 1. Workflow of mining for antimicrobial peptides embedded in protein sequences. (A) In nature, many peptides exert their biological functions after being proteolytically cleaved from precursor proteins. (B) By employing TransSAFP to mine functional peptide fragments from known protein sequences and chemical modifications, we discovered novel peptides with potential antimicrobial activity. SA represents self-assembling; AAs represent amino acids; and Glc represents glucose.

SAFP),[34] we identify candidate fragments embedded in natural proteins with predicted self-assembling propensity. Through amphiphilic modification and glycosylation, we further tune membrane selectivity and biocompatibility, thereby enhancing the ability of the candidate peptide to target the phosphatidylglycerol (PG) component of bacterial membranes and reducing the interaction with phosphatidylcholine (PC), the major lipid component of mammalian cell membranes. As a result, its selectivity index increased by approximately twofold. The resulting peptides form functional structures, eradicate biofilms, suppress resistance development, and exhibit therapeutic efficacy in murine infection models. This work illustrates how computational discovery combined with rational supramolecular design can convert latent protein fragments to potent antimicrobial assemblies. By bridging natural proteolytic principles with modern design tools, our study establishes a generalizable strategy for accessing hidden functional peptides in proteomes.

RESULTS AND DISCUSSION

Discovery of Self-Assembling Antimicrobial Peptides from Protein Sequences

To investigate whether latent antimicrobial fragments could be systematically mined from proteins, we applied a previously developed self-assembling peptide predictor (TransSAFP)[34] to a broadened set of proteins sourced from human, animal, and bacterial proteomes (Table S1). The protein sequences were randomly selected from these proteomes to ensure a diverse, nonbiased representation and include a broad range of annotated functions, such as antimicrobial and delivery-related activities, as well as uncharacterized proteins. The prediction results indicate heterogeneous scoring across both sequence fragments and N-terminal self-assembling moieties rather than a uniform trend (Figure S1 and Supplementary File 1). From this expanded protein set, TransSAFP identified 448 candidate self-assembling antimicrobial peptides (prediction >0.9). A subset of 16 peptides was randomly selected for synthesis and experimental validation. These peptides were subjected to purification (Figure S13 and S17-S31), followed by antimicrobial activity assays.

Experimental validation revealed that 15 peptides exhibited antimicrobial activity across the tested bacterial strains. Specifically, eight peptides were active against both representative Gram-negative (*E. coli* ATCC 25922 and *A. baumannii* BNCC 254392) and Gram-positive (*S. aureus* ATCC 25923 and MRSA USA 300) strains (MIC < 100 μg/mL). Two peptides were active against three strains, four peptides against two strains, and one peptide against a single strain (Figure 2 and Table S2). Several of the newly identified self-assembling antimicrobial peptides surpassed the activity of the parent proteins[35−41] (Table S3), illustrating how proteome-derived fragments can encode stronger antimicrobial functions than the full-length precursors from which they originate.

Importantly, the predictive framework was not limited to well-studied precursors. Five active peptides were identified from candidates predicted from uncharacterized proteins (140 candidates in total), supporting the concept that large fractions of proteomes may harbor cryptic antimicrobial assemblies that have remained unrecognized by conventional sequence analysis. These results, coupled with the 94% success rate in peptide validation, demonstrate that the TransSAFP mining pipeline provides a generalizable strategy for identifying functional self-assembling antimicrobial peptides across a broad range of proteomes.

These findings demonstrate that with the assistance of TransSAFP, novel self-assembling antimicrobial peptides with superior activity to the original proteins can be discovered from known sequences. Notably, TransSAFP is also capable of identifying active peptides from functionally uncharacterized proteins. Among the validated sequences, a minimal hexapeptide, KKFGKA (denoted as KA6), derived from magainin, proved especially potent. Upon N-terminal conjugation with a C_{16} aliphatic chain, KA6 exhibited robust activity across all four tested bacterial species, despite being the

https://doi.org/10.1021/jacs.5c20598
J. Am. Chem. Soc. 2026, 148, 4660−4669

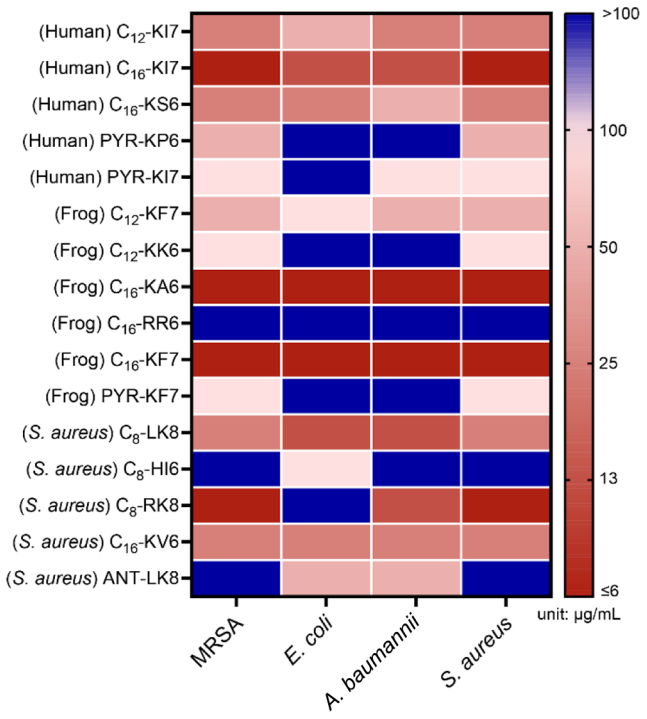

Figure 2. Identification of hidden antimicrobial peptides embedded in known protein sequences. MIC values of self-assembling antimicrobial peptides mined from protein sequences by TransSAFP.

shortest sequence in the series. This result underscores the dual importance of sequence-encoded assembly propensity and rational amphiphilic modification in producing short but powerful antimicrobial peptides. Together, these findings establish that systematic mining of proteomes can uncover short self-assembling fragments with unexpected antimicrobial activity, including from proteins with no known function. Moreover, the success of KA6 demonstrates that minimalistic fragments, once properly tuned, can achieve broad-spectrum potency while offering attractive advantages for synthesis and optimization.

Glycosylation Modulates Physicochemical Properties and Enhances Biocompatibility of C_{16}-KA6

We first evaluated the biocompatibility of lead C_{16}-KA6 through hemolysis and cytotoxicity assays. Despite its potent antimicrobial activity, C_{16}-KA6 induced significant hemolysis, with an HC_{50} of 60 μg/mL (selective index, SI = 10). In parallel, C_{16}-KA6 showed notable cytotoxicity toward 293T cells, with an IC_{50} of 42 μg/mL (SI = 7), yielding a narrow therapeutic window (Table S4). To overcome the limitations of the parent peptide, we introduced several monosaccharide moieties at the C-terminus of C_{16}-KA6, including glucosamine (Glc), mannosamine (Man), and galactosamine (Gal) (Figure 3A). The resulting glycosylated peptides (C_{16}-KA6-Glc, C_{16}-KA6-Man, and C_{16}-KA6-Gal; Figure S14−S16) were evaluated for their antimicrobial activity and biocompatibility. MIC assays demonstrated that all three glycosylated peptides retained broad-spectrum antimicrobial efficacy across four bacterial strains, with C_{16}-KA6-Glc exhibiting a modest overall advantage, particularly against *A. baumannii* (Table S4 and S5).

Hemolysis and cytotoxicity assays revealed that the glycosylation modifications enhanced the biocompatibility of C_{16}-KA6, with notable reductions in toxicity relative to the nonglycosylated peptide. Among the glycosylated variants, C_{16}-KA6-Glc showed the highest selectivity index (Table S4), confirming its balanced antimicrobial activity and improved therapeutic window. These findings demonstrate that glycosylation at the C-terminus provides an effective strategy for fine-tuning the biocompatibility and activity of proteome-derived peptides. Based on these results, we selected C_{16}-KA6-Glc as the optimized glycosylation for further studies, as it exhibited superior performance in both antimicrobial activity and biocompatibility. Overall, glycosylation not only improves the peptide's overall efficacy but also provides a generalizable approach for enhancing self-assembling antimicrobial peptides derived from proteomes.

Glycosylation altered several physicochemical parameters of the peptide.[42] LC spectra revealed a shift in the retention time from 4.00 to 3.87 min, consistent with increased hydrophilicity (Figure 3B). Critical aggregation concentration (CAC) measurements rose from 2 to 10 μg/mL (Figure 3C), indicating a reduced self-assembling propensity upon glycosylation. To further investigate the assembly structure, we performed a molecular dynamics (MD) simulation of C_{16}-KA6 and C_{16}-KA6-Glc. As shown in Figure S2 and S3, both peptides displayed a clear self-assembly tendency, as proved by the time-dependent decrease in the solvent-accessible surface area (SASA). Notably, the aggregation propensity (AP) value of C_{16}-KA6-Glc was lower than that of C_{16}-KA6, showing a reduced self-assembly propensity, which is consistent with the CAC results. MD snapshots at 150 ns (Figure 3E and F) revealed that C_{16} forms a hydrophobic core, while the peptide segments are distributed at the assembly surface, resulting in highly positively charged assemblies. In C_{16}-KA6-Glc assemblies, glucose moieties prefer to be distributed on the surface and partially shield cationic residues. Zeta potential analysis further showed that C_{16}-KA6-Glc assemblies carried a lower surface charge than did C_{16}-KA6 (Figure 3D), attributable to the exposure of hydrophilic glucose groups at the assembly interface, consistent with MD simulations. Despite these changes, dynamic light scattering (DLS) showed nearly overlapping correlation functions for the unmodified and glycosylated peptides, indicating that both assemble into structures of comparable hydrodynamic size (Figure S4). Consistent with this, transmission electron microscopy (TEM) confirmed that both peptides maintained a nanonet-like morphology (Figure S5, Figure 3G), suggesting that supramolecular organization remained intact.

We next compared the antimicrobial and biocompatibility profiles. Minimum inhibitory concentration (MIC) assays demonstrated that glycosylation did not compromise antibacterial potency: the MIC against MRSA remained unchanged at 6 μg/mL. In contrast, hemolysis and cytotoxicity were markedly reduced, with HC_{50} and IC_{50} values increasing more than 2-fold, to 163 and 87 μg/mL, respectively (Figure 3H,I). Consequently, the selective index improved substantially, to 27 and 15, greatly exceeding those of the nonglycosylated parent peptide (Figure 3J, Table S4). These results demonstrate that glycosylation selectively modulates peptide physicochemical properties—enhancing hydrophilicity, reducing aggregation tendency, and lowering surface charge—while preserving nanostructure and antimicrobial efficacy. This leads to significantly improved host compatibility and a broader therapeutic window. More broadly, the findings establish glycosylation as a generalizable chemical strategy for tuning the balance between potency and biocompatibility in

https://doi.org/10.1021/jacs.5c20598
J. Am. Chem. Soc. 2026, 148, 4660−4669

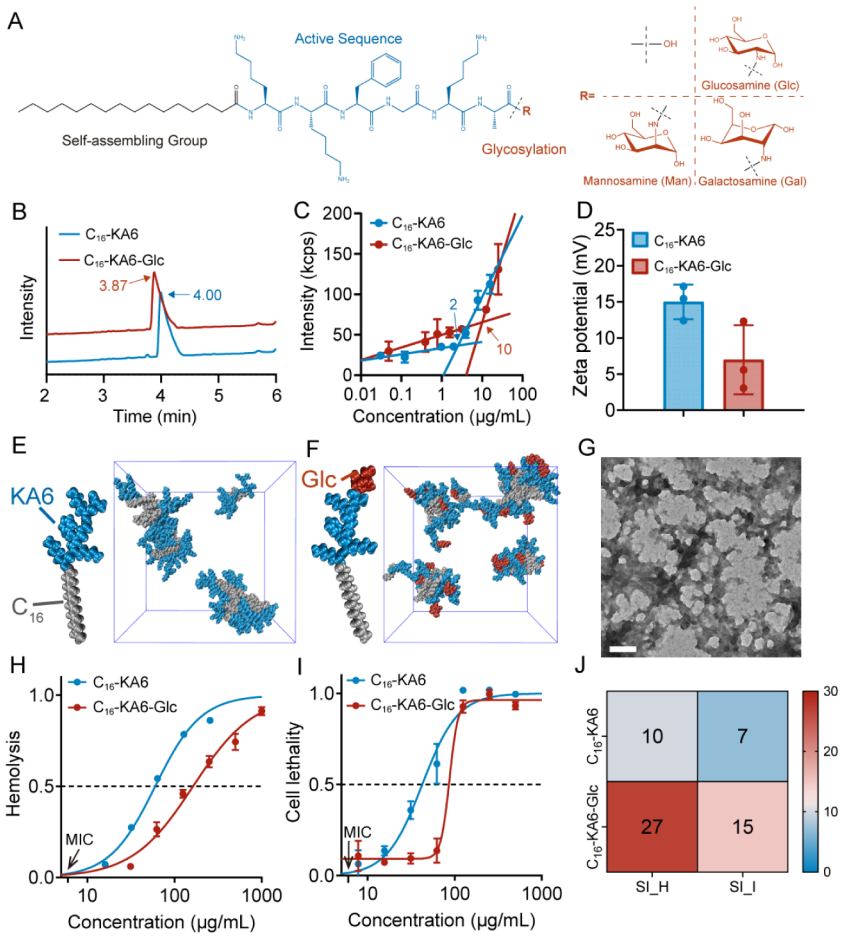

Figure 3. Glycosylation modulates the physicochemical properties, activity, and biocompatibility of the identified SAP. (A) Molecular structure of the optimized peptide (C_{16}-KA6-Glc) following TransSAFP prediction and wet-lab optimization. LC-MS spectra (B), CAC measurements (C), and zeta potential (D) of C_{16}-KA6 and C_{16}-KA6-Glc. Molecular dynamics (MD) simulations of C_{16}-KA6 (E) and C_{16}-KA6-Glc (F) assemblies. (G) TEM image of C_{16}-KA6-Glc at 5 × CAC. Scale bar, 100 nm. (H) Hemolytic effects of C_{16}-KA6 and C_{16}-KA6-Glc on RBCs. (I) Cytotoxicity of C_{16}-KA6 and C_{16}-KA6-Glc against 293T cells. (J) Selective index (SI) of C_{16}-KA6 and C_{16}-KA6-Glc. SI_H is calculated as the ratio of HC_{50} to the MIC, while SI_I is calculated as the ratio of IC_{50} to the MIC.

self-assembling antimicrobial peptides, consistent with previous reports.[43,44]

Bacterial Membrane Targeting of C_{16}-KA6-Glc

To elucidate the mechanism underlying its antimicrobial selectivity, we first used BioEM to examine the morphological changes in MRSA cells before and after exposure to C_{16}-KA6-Glc. Untreated MRSA exhibited intact cell membranes (Figure 4A). After the treatment of the peptide for 15 min, we observed that the peptide assemblies attached to the bacterial membrane (Figure 4B). Two hours incubation of the peptide led to significant membrane damage of cells, with peptide assemblies localized at disrupted regions and cytoplasmic leakage, resulting in bacterial death (Figure 4C).

We next investigated the membrane-targeting behavior of C_{16}-KA6-Glc using small unilamellar vesicle (SUV) models. Negatively charged bacterial membranes were mimicked with PC/PG vesicles (7:3 molar ratio), while mammalian membranes were represented by PC/Chol vesicles (1:1).[45] Encapsulation of 5(6)-carboxyfluorescein enabled leakage assays to monitor membrane disruption.[46] At its MIC, C_{16}-KA6-Glc induced ∼20% dye leakage from PC/PG vesicles, which increased in a concentration-dependent manner to ∼60% at 100 μg/mL (Figure 4D). By contrast, PC/Chol vesicles remained largely intact, with <5% leakage across the same range. DLS confirmed the size reduction of PC/PG vesicles upon treatment, consistent with disruption (Figure 4E), while zeta potential measurements revealed charge neutralization, supporting direct interaction between cationic peptide assemblies and negatively charged PG headgroups (Figure 4F). In contrast, for electrically neutral PC/Chol membranes, C_{16}-KA6-Glc treatment causes no detectable change in vesicle size or correlation function, indicating that the vesicles were unaffected (Figure S6). This observation is consistent with the fluorescence leakage assay results.

Competitive lipid binding assays reinforced this selectivity. Addition of PG to MRSA cultures elevated the MIC of C_{16}-KA6-Glc from 6 to 25 μg/mL at 50 μM PG and further to 200 μg/mL at 200 μM PG (Figure 4G). By contrast, cholesterol, PC, or PE did not affect activity. Given the potent activity of C_{16}-KA6-Glc against MRSA, vancomycin—a standard-of-care antibiotic for MRSA infections—was selected as a clinically relevant control. Vancomycin exerts its antibacterial effect by binding with high affinity to the D-Ala-D-Ala terminus of the cell wall precursor Lipid II,[47,48] thereby inhibiting peptidoglycan biosynthesis. Consequently, vancomycin activity is not influenced by the presence of free phospholipids, and no change in its MIC was observed upon the addition of

https://doi.org/10.1021/jacs.5c20598
J. Am. Chem. Soc. 2026, 148, 4660−4669

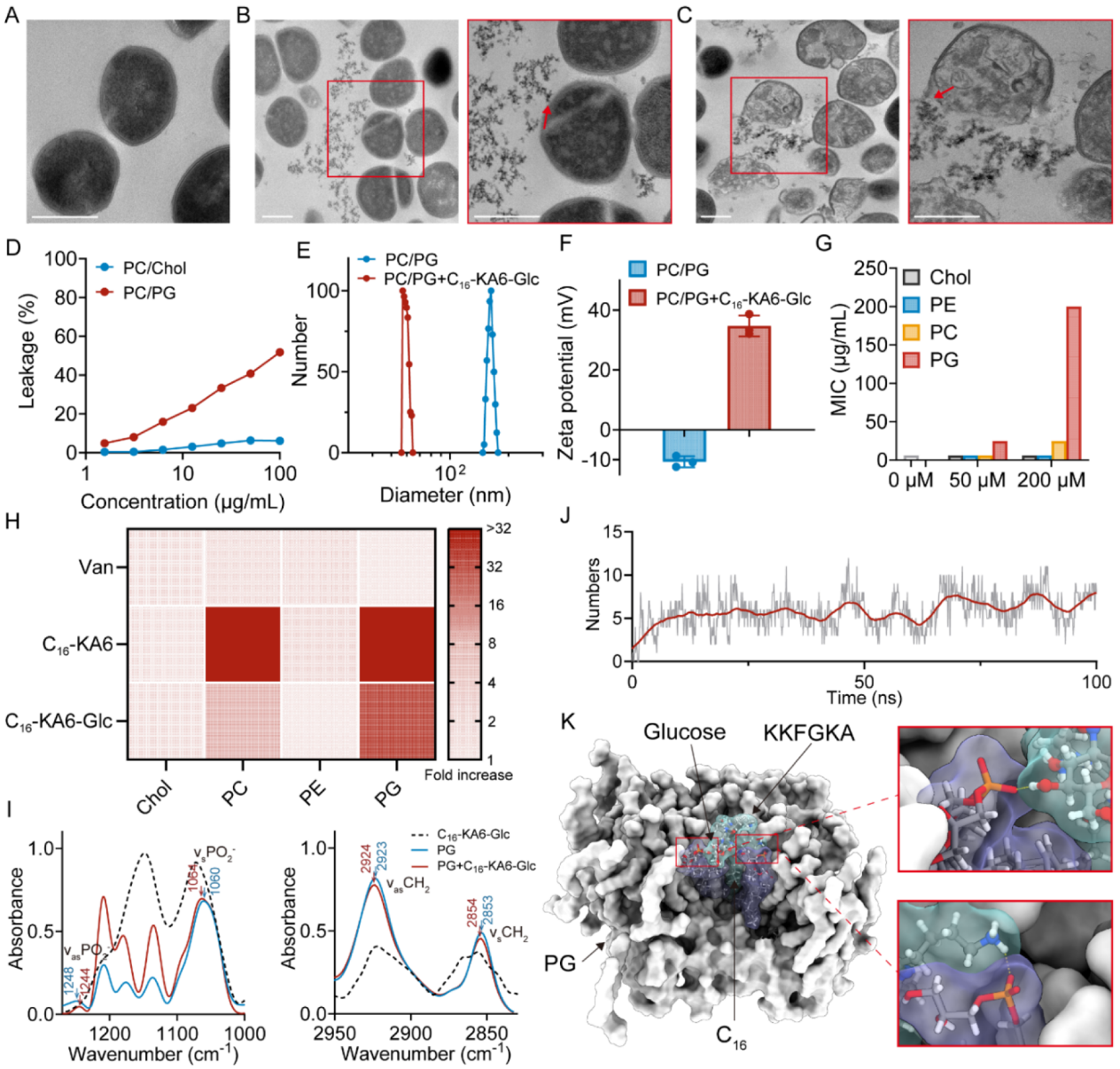

Figure 4. Interactions between C_{16}-KA6-Glc and phospholipid membrane components. BioEM images of MRSA cells without treatment (A) and after incubation with C_{16}-KA6-Glc for 15 min (B) and 2 h (C). Zoomed in views are marked by red boxes, and the red arrows highlight the sites where the peptide assemblies associate with the bacterial membrane. Scale bar: 500 nm. (D) Assessment of fluorescein leakage induced by C_{16}-KA6-Glc (2 h treatment) in uncharged SUVs (PC/Chol 1:1, 1 mM) and negatively charged SUVs (PC/PG 7:3, 1 mM). Size (E) and zeta potential (F) analyses of negatively charged SUVs before and after C_{16}-KA6-Glc treatment (100 μg/mL, 2 h). (G) MIC values of C_{16}-KA6-Glc against MRSA in the presence of membrane components. (H) Fold increase in MIC values of vancomycin (Van), C_{16}-KA6, and C_{16}-KA6-Glc against MRSA in the presence of membrane components. (I) FTIR analysis of DOPG vesicles (1 mM) after incubation with C_{16}-KA6-Glc (200 μg/mL) for 2 h. (J) Change of hydrogen bond number in MD simulation of the interaction between C_{16}-KA6-Glc and the PG bilayer. (K) Zoomed in view of MD simulation at 100 ns.

membrane lipid components (Figure 4H, Table S6). Importantly, while nonglycosylated C_{16}-KA6 exhibited a >32-fold MIC increase in the presence of both PG and PC—consistent with promiscuous targeting of bacterial and mammalian membranes—the glycosylated C_{16}-KA6-Glc displayed a 32-fold MIC increase only with PG, demonstrating its enhanced specificity for bacterial lipids. These findings are consistent with previous studies on PG-targeting antimicrobial agents[49−51] and further support that C_{16}-KA6-Glc targets PG, which explains its reduced hemolytic and cytotoxic effects. We subsequently performed molecular dynamics (MD) simulations to further investigate the interaction between C_{16}-KA6-Glc and the PG bilayer. As shown in Figure 4J, the number of hydrogen bonds between the peptide and the PG membrane increased over time and reached a plateau at approximately 100 ns. Analysis of the 100 ns snapshot reveals that the cationic residues and the hydrophilic glucose moiety preferentially associate with PG headgroups through hydrogen bonding, while the self-assembling C_{16} segment inserts into the hydrophobic core of the bilayer (Figure S8 and 4K). Notably, under identical simulation conditions, C_{16}-KA6-Glc formed a greater number of hydrogen bonds with the PG bilayer than the nonglycosylated C_{16}-KA6 (Figure S9), indicating that glycosylation enhances headgroup engagement. To exper-

https://doi.org/10.1021/jacs.5c20598
J. Am. Chem. Soc. 2026, 148, 4660−4669

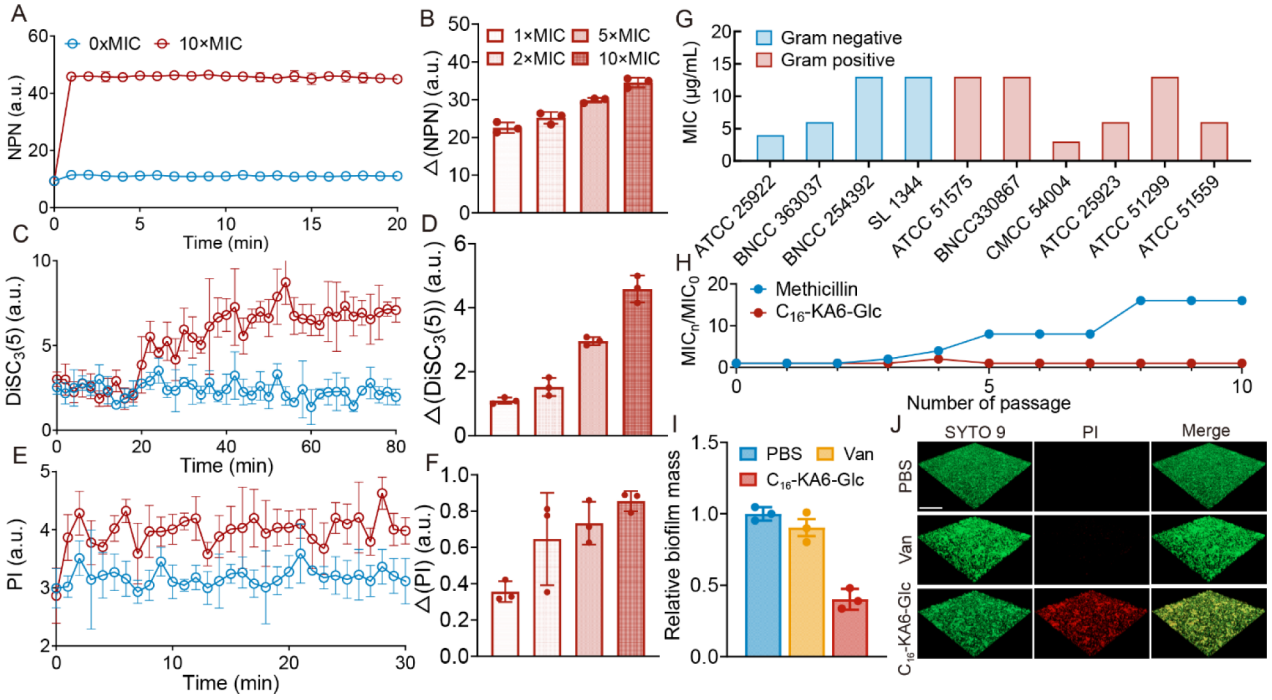

Figure 5. Effects of C_{16}-KA6-Glc on the bacterial membrane, its broad-spectrum antimicrobial activity, and biofilm eradication capacity. (A, B) Assessments of membrane disruption in MRSA induced by C_{16}-KA6-Glc using the NPN fluorescent probe. (C, D) Assessments of membrane depolarization in MRSA induced by C_{16}-KA6-Glc using the $DiSC_3(5)$ fluorescent probe. (E, F) Assessments of MRSA cell death induced by C_{16}-KA6-Glc using the PI fluorescent probe. (G) Broad-spectrum antimicrobial activity of C_{16}-KA6-Glc against various Gram-negative and Gram-positive bacteria. (H) Resistance development assays. MIC_0 represents the initial MIC value; MIC_n presents the MIC value after n passages. (I) Assessments of biofilm eradication abilities by crystal violet measurements. (J) CLSM images of the established MRSA biofilm treated with PBS, vancomycin (Van), and C_{16}-KA6-Glc at 20 × MIC, respectively. Scale bar: 100 μm.

imentally probe these interactions, we performed FTIR measurements using DOPG vesicles (Figure 4I). Upon incubation with C_{16}-KA6-Glc, the vibrational bands associated with the DOPG phosphate groups exhibited pronounced perturbations, indicating interaction with anionic PG headgroups.[52] In addition, shifts were observed in the spectral region corresponding to the DOPG acyl chains, which was consistent with hydrophobic insertion of the C_{16} moiety in the lipid bilayer. Taken together, the MD simulations and FTIR spectroscopy provide complementary, mutually consistent evidence that C_{16}-KA6-Glc engages PG membranes through a combination of electrostatic and hydrogen-bonding interactions with lipid headgroups coupled with hydrophobic insertion in the membrane interior. These findings support the membrane-selective mechanism of C_{16}-KA6-Glc and are consistent with its enhanced antibacterial activity and reduced cytotoxicity.

Bacterial membrane assays further showed that C_{16}-KA6-Glc rapidly perturbs the MRSA membranes. NPN uptake assays revealed concentration-dependent permeabilization (Figure 5A,B).[53] Complementary depolarization and integrity assays confirmed disruption of the membrane potential and compromise of the barrier function (Figure 5C−F). Traditional AMPs are often monomeric amphipathic peptides that disrupt membranes through direct insertion and pore formation, with activity and selectivity largely determined by net charge and amphipathicity.[54−56] By contrast, C_{16}-KA6-Glc functions as a supramolecular antimicrobial: amphiphilic modification drives self-assembly into nanoscale architectures that increase the multivalency and local peptide concentration at the bacterial membrane. This supramolecular organization, together with PG-preferential interactions at the assembly interface, enhances membrane selectivity and reduces mammalian membrane disruption. More broadly, self-assembly offers a generalizable chemical strategy to engineer potent yet selective antimicrobials by tuning assembly propensity and surface chemistry, rather than relying exclusively on sequence-level amphipathicity.

Broad-Spectrum Antimicrobial Activity and Biofilm Eradication Ability of C_{16}-KA6-Glc

We next evaluated the antimicrobial spectrum of C_{16}-KA6-Glc. Across 10 bacterial strains tested, including both Gram-positive and Gram-negative pathogens, all MIC values were ≤15 μg/mL, with five belonging to the ESKAPE group[57,58] (Figure 5G). This broad-spectrum activity underscores the utility of PG targeting as a unifying antimicrobial mechanism. Resistance development assays further revealed that repeated exposure to C_{16}-KA6-Glc did not increase the MIC of *S. aureus* over 10 serial passages, in stark contrast to methicillin, whose MIC increased 16-fold under the same conditions (Figure 5H). These results suggest that membrane-disruptive mechanisms based on PG targeting are inherently less prone to resistance development.

We also assessed antibiofilm activity against MRSA biofilms, where conventional antibiotics typically show limited efficacy. At 20 × MIC, C_{16}-KA6-Glc achieved ∼60% biofilm eradication, compared to <10% for vancomycin (Figure 5I). Confocal laser scanning microscopy (CLSM) confirmed these results, showing extensive bacterial killing within established biofilms treated with C_{16}-KA6-Glc, while vancomycin-treated biofilms remained largely intact (Figure 5J). Together, these results indicate that C_{16}-KA6-Glc exhibits broad-spectrum

https://doi.org/10.1021/jacs.5c20598
J. Am. Chem. Soc. 2026, 148, 4660−4669

antibacterial activity, a low propensity to induce resistance, and strong biofilm eradication capacity. These features are consistent with those reported for naturally discovered or rationally designed self-assembling antimicrobial peptides,[59−62] positioning it as a promising candidate for addressing infections that are recalcitrant to conventional antibiotics.

In Vivo Therapeutic Efficacy of C_{16}-KA6-Glc gainst MRSA Infection

To rigorously evaluate the therapeutic potential of C_{16}-KA6-Glc, we employed two complementary murine infection models that address distinct clinical contexts. The neutropenic thigh infection model eliminates host immune contributions, thereby directly testing the intrinsic bactericidal activity of a compound under conditions of severely compromised immunity. In contrast, the pneumonia model represents a physiologically complex and clinically relevant infection where bacterial aggregates and inflammatory tissue damage are central to pathogenesis. Together, these models provide a comprehensive assessment of both direct antimicrobial activity and the ability to modulate host responses.

Neutropenic Thigh Infection Model

Cyclophosphamide-induced neutropenia was established prior to MRSA inoculation into the thigh muscle (Figure 6A).

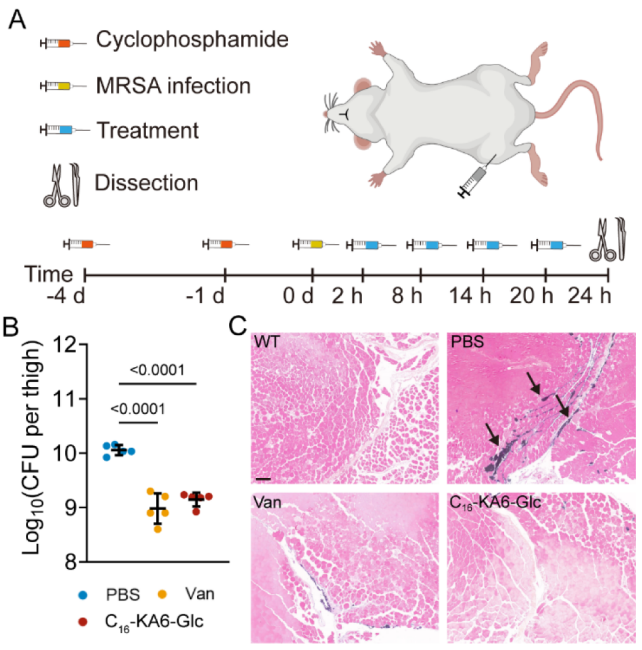

Figure 6. Therapeutic efficacy of C_{16}-KA6-Glc against MRSA-infected thigh. (A) The protocol of the in vivo therapeutic assay against the MRSA-infected thigh model. MRSA burden analysis (B) and Gram-staining analysis (C) of the thighs after different treatments. Scale bar, 100 μm. The arrows indicate regions of MRSA infection in the PBS group.

Subcutaneous administration of C_{16}-KA6-Glc every 6 h for four doses markedly reduced bacterial counts in infected tissue by approximately 90%, comparable to the efficacy of vancomycin treatment (Figure 6B). Histopathological analysis by Gram staining provided visual confirmation of these quantitative results (Figure 6C). In the PBS-treated controls, dense aggregates of MRSA cells were widely distributed. In contrast, Van- and C_{16}-KA6-Glc-treated tissues displayed markedly fewer or nearly absent MRSA colonies. The C_{16}-KA6-Glc-treated section closely resembled the uninfected WT control, showing no detectable Gram-positive staining. These results demonstrate that C_{16}-KA6-Glc achieves effective bacterial clearance comparable to that of vancomycin. Such efficacy under neutropenic conditions indicates that its bactericidal action is independent of host immune contribution, fulfilling a critical requirement for therapeutic application in immunocompromised hosts.

MRSA Pneumonia Model

We next tested efficacy in a lung infection model, where mice were intratracheally challenged with MRSA and treated 12 h postinfection, and then, tissues were collected at 36 h (Figure 7A). Both C_{16}-KA6-Glc and tobramycin (Tob) significantly reduced bacterial loads in lung tissue relative to the PBS group, showing an approximately 1-log reduction in CFU per lung (Figure 7B). Hematological results show that C_{16}-KA6-Glc treatment significantly reduced neutrophil and monocyte counts compared with PBS, indicating attenuation of systemic inflammation (Figure 7C,D). By contrast, tobramycin-treated mice retained elevated neutrophil levels. These data indicate that, in MRSA pneumonia, C_{16}-KA6-Glc therapy effectively lowers hematological indicators of inflammation. Histopathology further confirmed these protective effects. In PBS-treated lungs, H&E sections displayed pronounced alveolar wall thickening and interstitial inflammatory infiltrates, whereas both tobramycin and C_{16}-KA6-Glc treatments could attenuate these lung injuries (Figure 7G,H&E). Consistently, Gram staining revealed markedly reduced MRSA clusters after both treatments (Figure 7G, Gram). Immunohistochemistry further quantified the inflammatory response (Figure 7E−G). The IL-6 and LY6G positive area fractions were highest in PBS lungs and decreased significantly after tobramycin and C_{16}-KA6-Glc treatments. Notably, C_{16}-KA6-Glc achieved lower inflammatory indicator levels than did tobramycin. These results corroborated previous MRSA burden and hematological measurements. Collectively, these findings indicate that the C_{16}-KA6-Glc therapy matches tobramycin in MRSA clearance from the lung while exhibiting superior postclearance anti-inflammatory benefits, suggesting potential advantages for limiting infection-induced tissue injury.

Stability of C_{16}-KA6-Glc

We evaluated the stability of C_{16}-KA6-Glc against degradation by endogenous proteases, an important consideration for its potential development as a novel antimicrobial agent. HPLC analysis (Figure S11) showed that the C_{16}-KA6-Glc peak remains unchanged after incubation with 10% FBS for 4 h, indicating negligible degradation. However, even after 6 h, less than 10% of C_{16}-KA6-Glc had been hydrolyzed (Table S7). Consistently, the correlation-time plot (Figure S12) of the system containing C_{16}-KA6-Glc and FBS remained essentially unchanged, suggesting minimal variation in the hydrodynamic size of the assemblies in the system.

CONCLUSION

This work establishes a generalizable strategy for transforming latent protein fragments into therapeutic antimicrobial assemblies. By mining proteomes for self-assembling peptide fragments and refining their physicochemical properties through chemical design, we identified C_{16}-KA6-Glc as a minimalistic, yet potent, antimicrobial peptide. Glycosylation proved critical in reprogramming amphiphilic assemblies toward selective interaction with bacterial phosphatidylglycerol

https://doi.org/10.1021/jacs.5c20598
J. Am. Chem. Soc. 2026, 148, 4660−4669

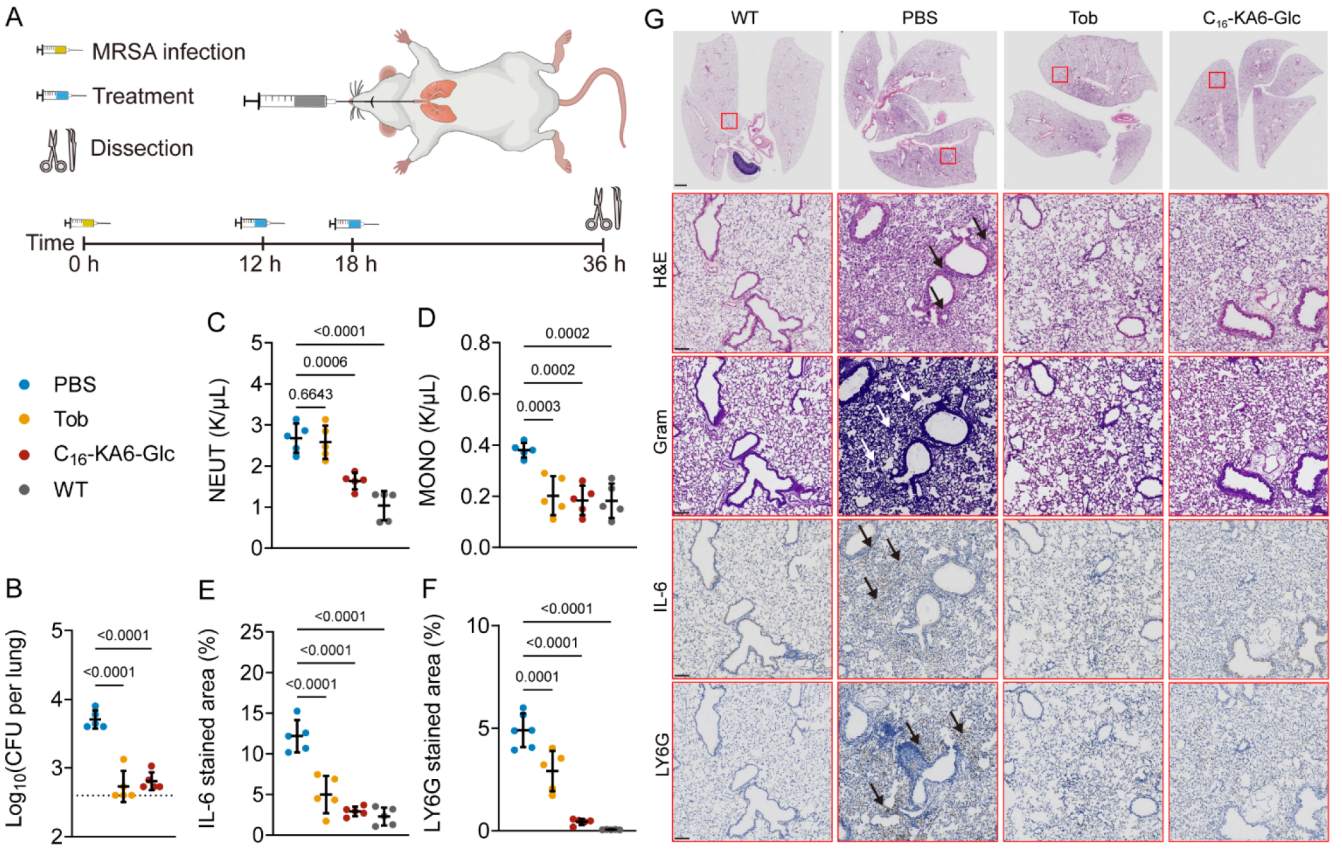

Figure 7. Therapeutic efficacy of C_{16}-KA6-Glc against MRSA-infected pneumonia. (A) The protocol of in vivo therapeutic assay against the MRSA-infected pneumonia model. (B) MRSA burden analysis. The dashed line indicates the detection limit. Hematological analysis (C, D) and histological analysis (E−G) after the treatment of different groups. (E, F) Quantification of positive staining areas from IL-6 and LY6G-stained results. (G) Lung tissue sections stained with H&E, Gram, IL-6, and LY6G. Enlarged H&E images (scale bar, 100 μm) are the red-marked area from the top-row H&E-stained tissue sections (scale bar, 1 mm). Other zoomed-in views of the same regions are from the corresponding Gram, IL-6, and LY6G-stained tissue sections (Figure S10). The arrows indicate regions of inflammatory cell infiltration in the H&E-stained sections, areas of MRSA infection in the Gram-stained sections, and IL-6 and LY6G positive regions in the corresponding IL-6 and LY6G-stained sections.

membranes while reducing toxicity to mammalian cells, thereby broadening the therapeutic window. Mechanistic studies demonstrated that C_{16}-KA6-Glc assembles into nanonets that permeabilize and depolarize bacterial membranes, with activity maintained across diverse pathogens. The peptide not only resisted the emergence of bacterial resistance but also eradicated established biofilms more effectively than conventional antibiotics. In two distinct infection models, C_{16}-KA6-Glc achieved therapeutic outcomes comparable to standard-of-care drugs while additionally attenuating inflammatory responses associated with infection. Beyond a single peptide, these findings illustrate how computational fragment mining coupled with supramolecular tuning can unlock the functional potential of proteome-encoded sequences. This approach bridges natural proteolytic strategies with modern design principles, offering a versatile framework for the discovery of next-generation antimicrobial peptides with built-in selectivity, resistance resilience, and host compatibility.

■ ASSOCIATED CONTENT

Supporting Information

The Supporting Information is available free of charge at https://pubs.acs.org/doi/10.1021/jacs.5c20598.

Prediction results collected in prediction results (XLSX)

Peptide synthesis and characterization, LC−MS spectra, TEM micrographs, MD simulation data, stability of the peptide, Gram, IL-6, LY6G staining images, MIC, HC_{50}, IC_{50}, and selectivity indices (PDF)

■ AUTHOR INFORMATION

Corresponding Author

Huaimin Wang − *State Key Laboratory of Gene Expression, School of Science, Westlake University, Hangzhou, Zhejiang 310024, China; Department of Chemistry, Westlake University, Hangzhou, Zhejiang 310024, China;* orcid.org/0000-0002-8796-0367; Email: wanghuaimin@westlake.edu.cn

Authors

Huayang Liu − *Department of Chemistry, Westlake University, Hangzhou, Zhejiang 310024, China*

Ziheng Xu − *State Key Laboratory of Gene Expression, School of Science, Westlake University, Hangzhou, Zhejiang 310024, China; Department of Chemistry, Westlake University, Hangzhou, Zhejiang 310024, China*

Yu Zhang − *Department of Chemistry, Westlake University, Hangzhou, Zhejiang 310024, China*

Dinghao Chen − *Department of Chemistry, Westlake University, Hangzhou, Zhejiang 310024, China*

https://doi.org/10.1021/jacs.5c20598
J. Am. Chem. Soc. 2026, 148, 4660−4669

Liheng Lu − *State Key Laboratory of Gene Expression, School of Science, Westlake University, Hangzhou, Zhejiang 310024, China; Department of Chemistry, Westlake University, Hangzhou, Zhejiang 310024, China*

Shichao Xu − *Department of Chemistry, Westlake University, Hangzhou, Zhejiang 310024, China*

Jianjun Cheng − *State Key Laboratory of Gene Expression, School of Science, Westlake University, Hangzhou, Zhejiang 310024, China; School of Engineering, Westlake University, Hangzhou, Zhejiang 310024, China;* orcid.org/0000-0003-2561-9291

Complete contact information is available at: https://pubs.acs.org/10.1021/jacs.5c20598

Author Contributions

‖H.L. and Z.X. contributed equally to this work.

Notes

The authors declare no competing financial interest.

■ ACKNOWLEDGMENTS

This work was supported by the National Natural Science Foundation of China (Grant No. U24A2076) and the "Pioneer"and "Leading Goose" R&D Program of Zhejiang (Grant 2025SDXHDX000*). We thank the Instrumentation and Service Center for Molecular Sciences, the Instrumentation and Service Center for Physical Sciences, the Biomedical Research Core Facilities, and the Supercomputer Center at Westlake University for technical assistance and access to instrumentation.

■ REFERENCES

(1) Tang, J.; Han, Z.; Sun, Y.; Zhang, H.; Gong, X.; Chai, J. Structural basis for recognition of an endogenous peptide by the plant receptor kinase PEPR1. *Cell Res.* **2015**, *25* (1), 110−120.

(2) Olsson, V.; Joos, L.; Zhu, S.; Gevaert, K.; Butenko, M. A.; De Smet, I. Look closely, the beautiful may be small: precursor-derived peptides in plants. *Annu. Rev. Plant Biol.* **2019**, *70* (1), 153−186.

(3) Sørensen, O. E.; Follin, P.; Johnsen, A. H.; Calafat, J.; Tjabringa, G. S.; Hiemstra, P. S.; Borregaard, N. Human cathelicidin, hCAP-18, is processed to the antimicrobial peptide LL-37 by extracellular cleavage with proteinase 3. *Blood* **2001**, *97* (12), 3951−3959.

(4) Sieprawska-Lupa, M.; Mydel, P.; Krawczyk, K.; Wójcik, K.; Puklo, M.; Lupa, B.; Suder, P.; Silberring, J.; Reed, M.; Pohl, J.; et al. Degradation of human antimicrobial peptide LL-37 by Staphylococcus aureus-derived proteinases. *Antimicrob. Agents Chemother.* **2004**, *48* (12), 4673−4679.

(5) Turner, J.; Cho, Y.; Dinh, N.-N.; Waring, A. J.; Lehrer, R. I. Activities of LL-37, a cathelin-associated antimicrobial peptide of human neutrophils. *Antimicrob. Agents Chemother.* **1998**, *42* (9), 2206−2214.

(6) Scott, M. G.; Davidson, D. J.; Gold, M. R.; Bowdish, D.; Hancock, R. E. The human antimicrobial peptide LL-37 is a multifunctional modulator of innate immune responses. *J. Immunol.* **2002**, *169* (7), 3883−3891.

(7) Bowdish, D. M.; Davidson, D. J.; Lau, Y. E.; Lee, K.; Scott, M. G.; Hancock, R. E. Impact of LL-37 on anti-infective immunity. *J. Leukocyte Biol.* **2004**, *77* (4), 451−459.

(8) Bowdish, D. M.; Davidson, D. J.; Scott, M. G.; Hancock, R. E. Immunomodulatory activities of small host defense peptides. *Antimicrob. Agents Chemother.* **2005**, *49* (5), 1727−1732.

(9) Weiss, M.; Steiner, D. F.; Philipson, L. H. Insulin biosynthesis, secretion, structure, and structure-activity relationships. In *Endotext*; MDText.com, Inc.: South Dartmouth, MA, 2015.

(10) Kemmler, W.; Peterson, J. D.; Steiner, D. F. Studies on the conversion of proinsulin to insulin: I. Conversion in vitro with trypsin and carboxypeptidase B. *J. Biol. Chem.* **1971**, *246* (22), 6786−6791.

(11) Júnior, N. G. O.; Souza, C. M.; Buccini, D. F.; Cardoso, M. H.; Franco, O. L. Antimicrobial peptides: structure, functions and translational applications. *Nat. Rev. Microbiol.* **2025**, *23*, 687−700.

(12) Zhang, Q. Y.; Yan, Z. B.; Meng, Y. M.; Hong, X. Y.; Shao, G.; Ma, J. J.; Cheng, X. R.; Liu, J.; Kang, J.; Fu, C. Y. Antimicrobial peptides: mechanism of action, activity and clinical potential. *Military Med. Res.* **2021**, *8* (1), 48.

(13) Dehsorkhi, A.; Castelletto, V.; Hamley, I. W. Self-assembling amphiphilic peptides. *J. Pept. Sci.* **2014**, *20* (7), 453−467.

(14) Feng, Z.; Wang, H.; Wang, S.; Zhang, Q.; Zhang, X.; Rodal, A. A.; Xu, B. Enzymatic assemblies disrupt the membrane and target endoplasmic reticulum for selective cancer cell death. *J. Am. Chem. Soc.* **2018**, *140* (30), 9566−9573.

(15) Feng, Z.; Wang, H.; Chen, X.; Xu, B. Self-assembling ability determines the activity of enzyme-instructed self-assembly for inhibiting cancer cells. *J. Am. Chem. Soc.* **2017**, *139* (43), 15377−15384.

(16) Ulijn, R. V.; Smith, A. M. Designing peptide based nanomaterials. *Chem. Soc. Rev.* **2008**, *37* (4), 664−675.

(17) Miller, S. E.; Tsuji, K.; Abrams, R. P.; Burke, T. R., Jr; Schneider, J. P. Uncoupling the folding-function paradigm of lytic peptides to deliver impermeable inhibitors of intracellular protein−protein interactions. *J. Am. Chem. Soc.* **2020**, *142* (47), 19950−19955.

(18) Smith, D. J.; Brat, G. A.; Medina, S. H.; Tong, D.; Huang, Y.; Grahammer, J.; Furtmüller, G. J.; Oh, B. C.; Nagy-Smith, K. J.; Walczak, P.; et al. A multiphase transitioning peptide hydrogel for suturing ultrasmall vessels. *Nat. Nanotechnol.* **2016**, *11* (1), 95−102.

(19) Su, H.; Zhang, W.; Wang, H.; Wang, F.; Cui, H. Paclitaxel-promoted supramolecular polymerization of peptide conjugates. *J. Am. Chem. Soc.* **2019**, *141* (30), 11997−12004.

(20) Ding, Y.; Zheng, D.; Xie, L.; Zhang, X.; Zhang, Z.; Wang, L.; Hu, Z.-W.; Yang, Z. Enzyme-instructed peptide assembly favored by preorganization for cancer cell membrane engineering. *J. Am. Chem. Soc.* **2023**, *145* (8), 4366−4371.

(21) Zheng, Z.; Chen, P.; Xie, M.; Wu, C.; Luo, Y.; Wang, W.; Jiang, J.; Liang, G. Cell environment-differentiated self-assembly of nanofibers. *J. Am. Chem. Soc.* **2016**, *138* (35), 11128−11131.

(22) Kim, J.; Lee, S.; Kim, Y.; Choi, M.; Lee, I.; Kim, E.; Yoon, C. G.; Pu, K.; Kang, H.; Kim, J. S. In situ self-assembly for cancer therapy and imaging. *Nat. Rev. Mater.* **2023**, *8* (11), 710−725.

(23) Hirschberg, J. K.; Brunsveld, L.; Ramzi, A.; Vekemans, J. A.; Sijbesma, R. P.; Meijer, E. Helical self-assembled polymers from cooperative stacking of hydrogen-bonded pairs. *Nature* **2000**, *407* (6801), 167−170.

(24) Jansen, S. A.; Weyandt, E.; Aoki, T.; Akiyama, T.; Itoh, Y.; Vantomme, G.; Aida, T.; Meijer, E. Simulating assembly landscapes for comprehensive understanding of supramolecular polymer−solvent systems. *J. Am. Chem. Soc.* **2023**, *145* (7), 4231−4237.

(25) Aida, T.; Meijer, E.; Stupp, S. Functional supramolecular polymers. *Science* **2012**, *335* (6070), 813−817.

(26) Wu, Q.; He, Z.; Wang, X.; Zhang, Q.; Wei, Q.; Ma, S.; Ma, C.; Li, J.; Wang, Q. Cascade enzymes within self-assembled hybrid nanogel mimicked neutrophil lysosomes for singlet oxygen elevated cancer therapy. *Nat. Commun.* **2019**, *10* (1), 240.

(27) Weng, J.; Huang, Z.; Liu, Y.; Wen, X.; Miao, Y.; Xu, J.-J.; Ye, D. Controlled in situ self-assembly of biotinylated trans-cyclooctene nanoparticles for orthogonal dual-pretargeted near-Infrared fluorescence and magnetic resonance imaging. *J. Am. Chem. Soc.* **2024**, *146* (19), 13163−13175.

(28) Kim, S.; Chae, J.-B.; Kim, D.; Park, C.-W.; Sim, Y.; Lee, H.; Park, G.; Lee, J.; Hong, S.; Jana, B.; et al. Supramolecular senolytics via intracellular oligomerization of peptides in response to elevated reactive oxygen species levels in aging cells. *J. Am. Chem. Soc.* **2023**, *145* (40), 21991−22008.

(29) Torres, M. D. T.; Wan, F.; de la Fuente-Nunez, C. Deep learning reveals antibiotics in the archaeal proteome. *Nat. Microbiol.* **2025**, *10*, 2153−2167.
(30) Diamond, G.; Beckloff, N.; Weinberg, A.; Kisich, K. O. The roles of antimicrobial peptides in innate host defense. *Curr. Pharm. Des.* **2009**, *15* (21), 2377−2392.
(31) Peschel, A.; Sahl, H.-G. The co-evolution of host cationic antimicrobial peptides and microbial resistance. *Nat. Rev. Microbiol.* **2006**, *4* (7), 529−536.
(32) Mookherjee, N.; Anderson, M. A.; Haagsman, H. P.; Davidson, D. J. Antimicrobial host defence peptides: functions and clinical potential. *Nat. Rev. Drug Discovery* **2020**, *19* (5), 311−332.
(33) Ma, Y.; Guo, Z.; Xia, B.; Zhang, Y.; Liu, X.; Yu, Y.; Tang, N.; Tong, X.; Wang, M.; Ye, X.; et al. Identification of antimicrobial peptides from the human gut microbiome using deep learning. *Nat. Biotechnol.* **2022**, *40* (6), 921−931.
(34) Liu, H.; Song, Z.; Zhang, Y.; Wu, B.; Chen, D.; Zhou, Z.; Zhang, H.; Li, S.; Feng, X.; Huang, J.; et al. De novo design of self-assembling peptides with antimicrobial activity guided by deep learning. *Nat. Mater.* **2025**, *24* (8), 1295−1306.
(35) Mechesso, A. F.; Su, Y.; Xie, J.; Wang, G. Enhanced antimicrobial screening sensitivity enabled the identification of an ultrashort peptide KR-8 for engineering of LL-37mini to combat drug-resistant pathogens. *ACS Infect. Dis.* **2023**, *9* (11), 2215−2225.
(36) Strömstedt, A. A.; Park, S.; Burman, R.; Göransson, U. Bactericidal activity of cyclotides where phosphatidylethanolamine-lipid selectivity determines antimicrobial spectra. *Biochim. Biophys. Acta* **2017**, *1859* (10), 1986−2000.
(37) Feng, X.; Sambanthamoorthy, K.; Palys, T.; Paranavitana, C. The human antimicrobial peptide LL-37 and its fragments possess both antimicrobial and antibiofilm activities against multidrug-resistant Acinetobacter baumannii. *Peptides* **2013**, *49*, 131−137.
(38) Yan, H.; Hancock, R. E. Synergistic interactions between mammalian antimicrobial defense peptides. *Antimicrob. Agents Chemother.* **2001**, *45* (5), 1558−1560.
(39) Shin, A.; Lee, E.; Jeon, D.; Park, Y.-G.; Bang, J. K.; Park, Y.-S.; Shin, S. Y.; Kim, Y. Peptoid-substituted hybrid antimicrobial peptide derived from papiliocin and magainin 2 with enhanced bacterial selectivity and anti-inflammatory activity. *Biochemistry* **2015**, *54* (25), 3921−3931.
(40) Glattard, E.; Salnikov, E. S.; Aisenbrey, C.; Bechinger, B. Investigations of the synergistic enhancement of antimicrobial activity in mixtures of magainin 2 and PGLa. *Biophys. Chem.* **2016**, *210*, 35−44.
(41) Cirioni, O.; Silvestri, C.; Ghiselli, R.; Giacometti, A.; Orlando, F.; Mocchegiani, F.; Chiodi, L.; Vittoria, A. D.; Saba, V.; Scalise, G. Experimental study on the efficacy of combination of α-helical antimicrobial peptides and vancomycin against Staphylococcus aureus with intermediate resistance to glycopeptides. *Peptides* **2006**, *27* (11), 2600−2606.
(42) Yuan, D.; Shi, J.; Du, X.; Zhou, N.; Xu, B. Supramolecular glycosylation accelerates proteolytic degradation of peptide nanofibrils. *J. Am. Chem. Soc.* **2015**, *137* (32), 10092−10095.
(43) Bednarska, N. G.; Wren, B. W.; Willcocks, S. J. The importance of the glycosylation of antimicrobial peptides: natural and synthetic approaches. *Drug Discovery Today* **2017**, *22* (6), 919−926.
(44) Li, W.; Separovic, F.; O'Brien-Simpson, N. M.; Wade, J. D. Chemically modified and conjugated antimicrobial peptides against superbugs. *Chem. Soc. Rev.* **2021**, *50* (8), 4932−4973.
(45) Fa, K.; Liu, H.; Gong, H.; Zhang, L.; Liao, M.; Hu, X.; Ciumac, D.; Li, P.; Webster, J.; Petkov, J.; et al. In-membrane nanostructuring of cationic amphiphiles affects their antimicrobial efficacy and cytotoxicity: a comparison study between a de novo antimicrobial lipopeptide and traditional biocides. *Langmuir* **2022**, *38* (21), 6623−6637.
(46) Fa, K.; Liu, H. Y.; Li, Z. Y.; Gong, H. N.; Petkov, J.; Lu, J. R. Acyl chain length tuning improves antimicrobial potency and biocompatibility of short designed lipopeptides. *J. Colloid Interface Sci.* **2023**, *630*, 911−923.
(47) Gardete, S.; Tomasz, A. Mechanisms of vancomycin resistance in Staphylococcus aureus. *J. Clin. Invest.* **2014**, *124* (7), 2836−2840.
(48) Stogios, P. J.; Savchenko, A. Molecular mechanisms of vancomycin resistance. *Protein Sci.* **2020**, *29* (3), 654−669.
(49) Liang, Y.; Zhang, Y.; Huang, Y.; Xu, C.; Chen, J.; Zhang, X.; Huang, B.; Gan, Z.; Dong, X.; Huang, S. Helicity-directed recognition of bacterial phospholipid via radially amphiphilic antimicrobial peptides. *Sci. Adv.* **2024**, *10* (35), No. eadn9435.
(50) Chen, X.; Song, M.; Tian, L.; Shan, X.; Mao, C.; Chen, M.; Zhao, J.; Sami, A.; Yin, H.; Ali, U.; et al. A plant peptide with dual activity against multidrug-resistant bacterial and fungal pathogens. *Sci. Adv.* **2025**, *11* (12), No. eadt8239.
(51) Zhang, X.; Luo, D.; Xia, R.; Wu, K.; Li, X.; Chen, J.; Zhou, H.; Hu, J.; Huang, S.; Jia, S.; et al. Bacterial Phospholipid-Inducible Helix-Transformable Antimicrobial Polypeptides. *J. Am. Chem. Soc.* **2025**, *147* (45), 41800−41808.
(52) El Battioui, K.; Chakraborty, S.; Wacha, A.; Molnár, D.; Quemé-Peña, M.; Szigyártó, I. C.; Szabó, C. L.; Bodor, A.; Horvati, K.; Gyulai, G.; et al. In situ captured antibacterial action of membrane-incising peptide lamellae. *Nat. Commun.* **2024**, *15* (1), 3424.
(53) Torres, M. D.; Melo, M. C.; Flowers, L.; Crescenzi, O.; Notomista, E.; de la Fuente-Nunez, C. Mining for encrypted peptide antibiotics in the human proteome. *Nat. Biomed. Eng.* **2022**, *6* (1), 67−75.
(54) Matsuzaki, K.; Murase, O.; Miyajima, K. Kinetics of pore formation by an antimicrobial peptide, magainin 2, in phospholipid bilayers. *Biochemistry* **1995**, *34* (39), 12553−12559.
(55) Song, C.; Weichbrodt, C.; Salnikov, E. S.; Dynowski, M.; Forsberg, B. O.; Bechinger, B.; Steinem, C.; De Groot, B. L.; Zachariae, U.; Zeth, K. Crystal structure and functional mechanism of a human antimicrobial membrane channel. *Proc. Int. Acad. Ecol. Environ. Sci.* **2013**, *110* (12), 4586−4591.
(56) Lee, C.-C.; Sun, Y.; Qian, S.; Huang, H. W. Transmembrane pores formed by human antimicrobial peptide LL-37. *Biophys. J.* **2011**, *100* (7), 1688−1696.
(57) Santajit, S.; Indrawattana, N. Mechanisms of antimicrobial resistance in ESKAPE pathogens. *BioMed. Res. Int.* **2016**, *1*, 2475067.
(58) De Oliveira, D. M. P.; Forde, B. M.; Kidd, T. J.; Harris, P. N. A.; Schembri, M. A.; Beatson, S. A.; Paterson, D. L.; Walker, M. J. Antimicrobial resistance in ESKAPE pathogens. *Clin. Microbiol. Rev.* **2020**, *33* (3), 10−1128.
(59) Ouellette, A. J.; Selsted, M. E. Immunology. HD6 defensin nanonets. *Science* **2012**, *337* (6093), 420−421.
(60) Li, R. S.; Liu, J. H.; Wen, C.; Shi, Y. R.; Ling, J.; Cao, Q.; Wang, L.; Shi, H.; Huang, C. Z.; Li, N. Transformable nano-antibiotics for mechanotherapy and immune activation against drug-resistant Gram-negative bacteria. *Sci. Adv.* **2023**, *9* (34), No. eadg9601.
(61) Fan, Y.; Li, X. -D.; He, P. -P.; Hu, X. -X.; Zhang, K.; Fan, J. -Q.; Yang, P. -P.; Zheng, H. -Y.; Tian, W.; Chen, Z. -M.; et al. A biomimetic peptide recognizes and traps bacteria in vivo as human defensin-6. *Sci. Adv.* **2020**, *6* (19), No. eaaz4767.
(62) Huang, Z.; Liu, Y.; Wang, L.; Ali, A.; Yao, Q.; Jiang, X.; Gao, Y. Supramolecular assemblies mimicking neutrophil extracellular traps for MRSE infection control. *Biomaterials* **2020**, *253*, 120124.

https://doi.org/10.1021/jacs.5c20598
J. Am. Chem. Soc. 2026, 148, 4660−4669